A physiologically based model of bile acid metabolism in mice.

Bastian Kister[1,2], Alina Viehof[3], Ulrike Rolle-Kampczyk[4], Annika Schwentker[5], Nicole Simone Treichel[3], Susan Jennings[3], Theresa H. Wirtz[6], Lars M. Blank[2], Mathias W. Hornef[5], Martin von Bergen[4], Thomas Clavel[3], Lars Kuepfer[1],

1 Institute for Systems Medicine with Focus on Organ Interaction, University Hospital RWTH Aachen, Aachen, Germany.
2 Institute of Applied Microbiology, RWTH Aachen, Aachen, Germany.
3 Functional Microbiome Research Group, Institute of Medical Microbiology, University Hospital RWTH Aachen, Aachen, Germany.
4 Department of Molecular Systems Biology, Helmholtz Centre for Environmental Research (UFZ), Leipzig, Germany.
5 Institute of Medical Microbiology, University Hospital RWTH Aachen, Aachen, Germany.
6 Department of Medicine III, University Hospital RWTH Aachen, Aachen, Germany.

Abstract

Bile acid (BA) metabolism is a complex system that encompasses a diverse mixture of primary and secondary, as well as conjugated and unconjugated BAs that undergo continuous enterohepatic circulation (EHC). Alterations in both composition and dynamics of BAs have been associated with various diseases; however, a mechanistic understanding of the relationship between altered BAs metabolism and related diseases is lacking. Computational modeling may support functional analyses of the physiological processes involved in the EHC of bile acids along gut the gut-liver axis. In this study, we developed a physiology-based model of murine BA metabolism describing synthesis, conjugation, microbial transformations, systemic distribution, excretion and EHC of BAs as well as an explicit representation of the host physiology at the whole-body level. For model development, BA metabolism of specific pathogen-free (SPF) was characterized in vivo by measuring BA levels and composition in various organs, expression of transporters along the gut and cecal microbiota composition. Interestingly, We found significantly different BA levels between male and female mice that could only be explained by adjusted expression of the hepatic enzymes and transporters in the model. Of note, this finding was in agreement with earlier experimental observations. The model for SPF mice could also describe equivalent experimental data in germ-free mice by specifically switching of microbial activity in the intestine. The here presented model hence allows functional analysis of BA metabolism in mice. In the future, the model may support the translation of results from mouse studies to a clinically relevant context through cross-species extrapolation.

Introduction

Bile acids are involved in many physiological processes in the body including hormone metabolism or digestion of nutrients [1, 2]. The bile acid (BA) pool is a complex

mixture of different BA species. Primary BAs are synthesized from cholesterol within the liver and are converted to various secondary BAs by the intestinal microbiome [3]. BAs are furthermore conjugated with either glycine or taurine in hepatocytes.

Within the body, BAs continuously undergo enterohepatic circulation (EHC) between the liver and the intestine along the gut-liver axis. Hepatic BAs are secreted into the bile canaliculi and accumulate in the gallbladder. Upon food intake, gallbladder contractions release large amounts of the stored BAs into the small intestine, where they are transported along the gut. Most BAs are actively taken up by enterocytes, predominantly in the ileum, and further excreted towards portal blood. The remaining proportion is subject to microbial transformations, especially in the colon. BAs are then either taken up by passive diffusion or they are secreted with the feces. From the portal blood, BAs are efficiently reabsorbed into the liver. Through sinusoidal transport they may subsequently reach the vascular circulation and eventually other tissues.

Due to the systemic nature of bile acid metabolism, diseases of both the liver (e.g. liver cirrhosis, liver cancer or inflammatory bowel disease) and the intestine (e.g. ulcerative colitis or Crohn's Disease) have been associated with alterations in BA composition and distribution [2, 4–11]. Such changes, however, may be difficult to investigate due to the complexity of the processes involved.

In this work, we developed a physiologically-based pharmacokinetic (PBPK) model of murine BA metabolism at the whole-body level which may be used as a platform for mechanistic investigation of BA metabolism. This model is of particular interest since mice are the most commonly utilized animal model to investigate human metabolism [12, 13]. Mice produce cholic acid (CA) as well as muricholic acids (MCAs) that are made from chenodeoxycholic acid (CDCA). MCAs are hydroxylated at the C-6 position, which alters their physicochemical as well as the signalling properties. MCAs are more hydrophilic and less cytotoxic than other BAs and function as FXR antagonists instead of activating FXR signalling like other BAs [14]. .

Our model describes the physiology of murine bile acid metabolism at a large level of detail and can be used to simulate tissue concentration profiles of the most abundant BAs in mice. To inform the model, mice were characterized concerning their BA composition in various organs, their BA transporter expression along the gut axis and their cecal microbiota composition. Our model was further validated to complementary data set generated from germ-free mice. The here presented model may further serve as a tool for hypothesis testing and as a bridge between discoveries within mouse studies and clinical applications in human patients.

Results

A Physiologically-Based Model of Bile Acid Metabolism

The physiology-based murine model of BA metabolism includes synthesis, hepatic and microbial transformations, circulation and excretion of BAs (Figure 1). For model development we used a PBPK model [15] in which BA metabolites were considered as the circulating molecules. The basic PBPK model represents the physiology of mice at a large level of detail. It therefore includes a significant amount of prior physiological knowledge regarding organ volumes, tissue composition, organ surface areas or blood perfusion rates [**?**, 16]. Of note, the extrapolation to new scenarios and conditions is well possible due to the mechanistic structure of the underlying PBPK model [17, 18].

In order to specifically inform physiological and kinetic parameters for bile acid metabolism in mice, an extensive experimental data collection was performed. This data comprised measurements of BA level and composition in different tissues of specific pathogen free (SPF) mice (Figure 2), physiological parameters (Figure 3),

quantification of transporter gene expression in different segments of the gut as well as the cecal microbiome composition (Figure 4).

An initial screening of BA levels showed that female mice have in general higher levels of BAs than their male littermates which is in agreement with published studies [19]. In our data, BA concentration in female mice was consistently increased in venous blood plasma, liver, bile and intestinal tissues (Figure 2A-E,I,K,L). Levels in the gut lumen were higher in the small intestine (Figure 2F,H), while the content of the large intestine did not show a clear picture (Figure 2J,M). Only in the ileal tissue, male mice displayed higher concentration of BAs than female mice (Figure 2G).

In order to account for sex-related variation in BA metabolism we hence decided to built separate physiologically based models for male and female SPF mice. Using physiology-based modeling for describing bile acid metabolism enabled us to incorporate explicit information on the organism's physiology (Figure 3. In this study, male mice were approx. 30% heavier (Figure 3A), and correspondingly in female mice the liver and kidney were smaller; however the latter being disproportionately so (Figure 3C). Interestingly, the intestine had approximately the same length regardless of sex; thus, female mice showed a longer intestine compared to their body weight (Figure 3B).

Four transport processes were furthermore considered in the model: (1) Excretion of BAs from the liver into the duodenum by the bile salt export pump (BSEP), (2) uptake from the gut lumen by the apical sodium-dependent bile acid transporter (ASBT), (3) excretion from enterocytes to portal blood by the organic solute and steroid transporter (OSTα/β) and (4) uptake of BAs from portal blood into hepatocytes by the sodium/taurocholate cotransporting polypeptide (NTCP). Expression of the transporters (ASBT, OSTα/β) along the gut axis showed overall no differences between male and female mice; however, they varied strongly between different gut segments (Figure 4A).

To examine potential differences in the microbiome of male and female mice, the microbial composition within the cecum was analyzed. First, we determined α-diversity for the within-sample taxonomic diversity. The determined species richness, as well as the Shannon effective index, showed no significant sex-related difference (Figure 4B). Similarities in microbial community structure (β-diversity) were assessed based on generalized UniFrac distances. We observed no clear separation of mice based on sex and overall high similarity between all samples (Figure 4C).

In contrast, we found significant differences in the relative abundance of two bacterial genera between male and female mice. In female mice, Lachnospiraceae UCG-006 was more abundant, whereas an unknown genus of the Muribaculacea family was more prominent in male mice (Figure 4D). However, no information was available linking either genera to BA metabolism. Overall, these results indicate that there are no relevant differences in intestinal transporter expression and microbiota composition between male and female mice.

Besides the aforementioned physiology of the organism, physicochemical properties such as molecular weight, solubility, lipophilicity (logP) and plasma-protein binding (fraction unbound) are a second important pillar of PBPK models [15]. Organ-plasma partitioning and passive transport can be directly derived from these parameters using an appropriate distribution model. For the physiology-based model of bile acid metabolism, physicochemical properties of the tauro-conjugated forms (Table 1) were used to inform the compound properties of the PBPK model for small molecules.

In the computational model, total levels of CA, MCAs, CDCA, DCA, UDCA and LCA were considered as these represent the most abundant BAs that could also be measured in all compartments. De novo synthesis of BAs was considered as a constant formation rate in the intracellular space of the liver, and its magnitude was estimated from the excretion rate in feces [20–22] and urine [23]. Both excretion processes were

considered by passive transport or active clearance, respectively. Subsequent formation of MCA using CDCA or UDCA as well as hepatic DCA hydroxylation was included in the model. Microbial metabolism of BAs was modeled as net enzymatic reactions, and the relative abundance of the corresponding enzymes along the gut was correlated with the activity of bile salt hydrolase (BSH) [24]. Reactions included were dehydroxylation of CA, CDCA and UDCA to DCA, LCA and UDCA (Figure 1).

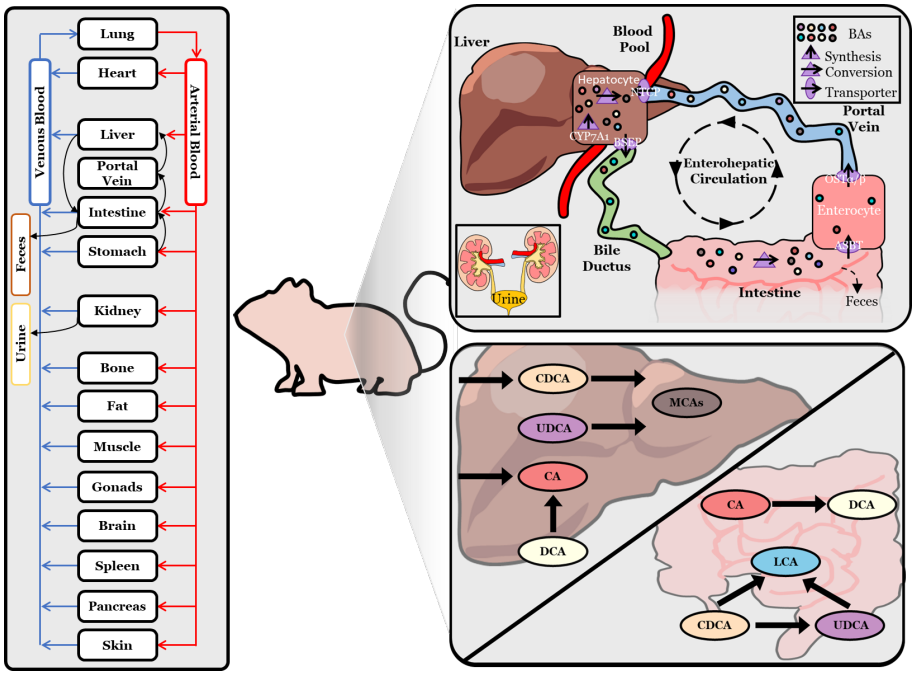

Fig 1. Physiology-based bile acid model. Schematic overview of a PBPK model of bile acid biosynthesis via CYP7A1, hepatic and microbial transformation, active transport processes via BSEP, ASBT, OST-α/β and NTCP, as well as fecal and renal excretion. Excretion to the gallbladder is neglected and BAs are directly secreted into the duodenum. Reactions of BAs are located either in the intracellular space of the liver or in the intestinal lumen.

Table 1. Physicochemical properties of bile acids used.

BA species	Used as	Property	Value	Source
T-CA	tCA	MW [g/mol]	515.7	PubChem Identifier: CID 6675
T-CA	tCA	Solubility [g/l]	0.077	ALOGPS (HMDB [25])
T-CA	tCA	logP	0	Heuman et al. [26]
T-CA	tCA	pKa (acidic)	-0.88	ChemAxon (HMDB [25])
T-CA	tCA	pKa (basic)	-0.053	ChemAxon (HMDB [25])
T-CA	tCA	FU	0.359	Predicted [27]
T-CDCA	tCDCA	MW [g/mol]	499.7	PubChem Identifier: CID
T-CDCA	tCDCA	Solubility [g/l]	0.00748	ALOGPS (HMDB [25])
T-CDCA	tCDCA	logP	0.46	Heuman et al. [26]
T-CDCA	tCDCA	pKa (acidic)	-0.99	ChemAxon (HMDB [25])
T-CDCA	tCDCA	pKa (basic)	0.18	ChemAxon (HMDB [25])
T-CDCA	tCDCA	FU	0.0776	Predicted [27]
T-UDCA	tUDCA	MW [g/mol]	499.7	PubChem Identifier: CID 9848818
T-UDCA	tUDCA	Solubility [g/l]	0.0075	ALOGPS (HMDB [25])
T-UDCA	tUDCA	logP	-0.94	Heuman et al. [26]
T-UDCA	tUDCA	pKa (acidic)	-0.99	ChemAxon (HMDB [25])
T-UDCA	tUDCA	pKa (basic)	0.18	ChemAxon (HMDB [25])
T-UDCA	tUDCA	FU	0.0776	Predicted [27]
T-DCA	tDCA	MW [g/mol]	499.7	PubChem Identifier: CID 2733768
T-DCA	tDCA	Solubility [g/l]	0.0078	ALOGPS (HMDB [25])
T-DCA	tDCA	logP	0.59	Heuman et al. [26]
T-DCA	tDCA	pKa (acidic)	-0.75	ChemAxon (HMDB [25])
T-DCA	tDCA	pKa (basic)	-0.2	ChemAxon (HMDB [25])
T-DCA	tDCA	FU	0.0768	Predicted [27]
T-LCA	tLCA	MW [g/mol]	483.7	PubChem Identifier: CID 439763
T-LCA	tLCA	Solubility [g/l]	0.00028	ALOGPS (HMDB [25])
T-LCA	tLCA	logP	1	Heuman et al. [26]
T-LCA	tLCA	pKa (acidic)	-0.63	ChemAxon (HMDB [25])
T-LCA	tLCA	pKa (basic)	-1.1	ChemAxon (HMDB [25])
T-LCA	tLCA	FU	0.0618	Predicted [27]
T-MCA	tMCA	MW [g/mol]	515.7	PubChem Identifier: CID 168408
T-MCA	tMCA	Solubility [g/l]	0.075	ALOGPS (HMDB [25])
T-MCA	tMCA	logP	-0.81	Heuman et al. [26]
T-MCA	tMCA	pKa (acidic)	-0.98	ChemAxon (HMDB [25])
T-MCA	tMCA	pkA (basic)	0.084	ChemAxon (HMDB [25])
T-MCA	tMCA	FU	0.365	Predicted [27]

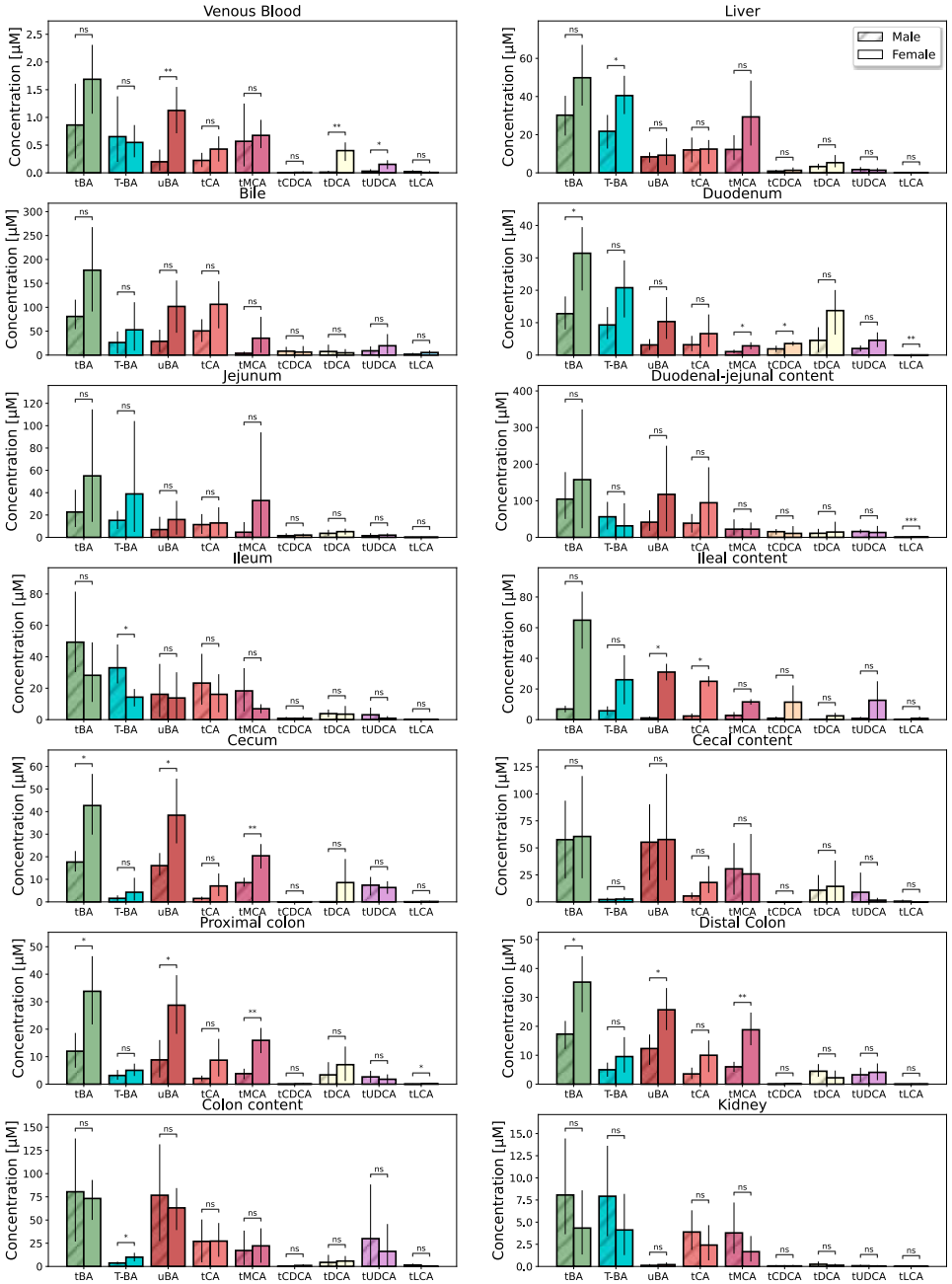

Fig 2. Bile acid levels in SPF mice. Concentration of total BAs (tBA), tauro-conjugated BAs (T-BA), unconjugated BA (uBA), total cholic acid (tCA), total muricholic acids (tMCA), total chenodeoxycholic acid (tCDCA), total deoxycholic acid (tDCA), total ursodeoxycholic acid (tUDCA) and total lithocholic acid (tLCA) in various organs in male and female SPF mice. Statistical differences were assessed by independent t-test. Statistical significance is marked with asterisks.

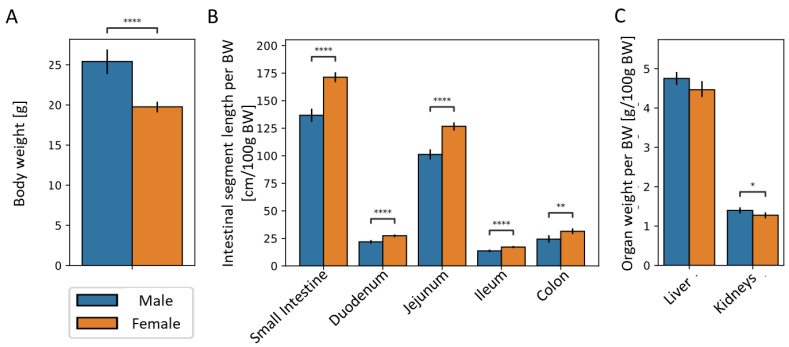

Fig 3. Physiological differences between male and female mice. Assessment of sex-related differences in body weight (A), length of intestinal segments (B) as well as weight of the liver and the kidneys (C) in SPF mice. Significant differences were tested by two-way, independent t-test and significance was marked with asterisks.

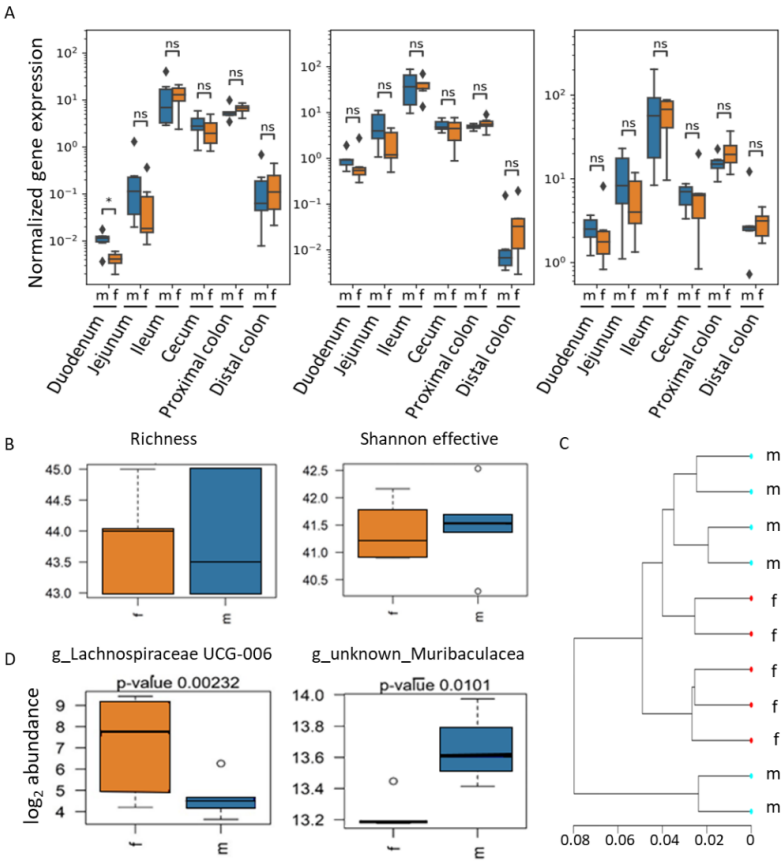

Fig 4. Sex-related differences in intestinal BA metabolism. Assessment of sex-related differences in the intestine relevant to BA metabolism: A) Expression of the BA transporters ASBT, OST-α and OST-β (from left to right) along the gut axis in male and female SPF mice measured by qPCR. Statistical significance was assessed by Mann-Whitney U-test and statistical significance is marked with asterisks. B) Analysis of the cecal microbiome in male and female SPF mice by assessing observed species richness and Shannon effective index as indices of α-diversity, and C) β-diversity by hierarchical clustering of samples. D) The $\log_2$ abundance of genera, which significantly differed between male and female mice. Statistical significance was determined using Wald test ($\alpha = 0.05$).

Model calibration to data from SPF mice

For parameter estimation, we allowed sex-related differences in active hepatic processes. By doing so, we found that downregulation of BA synthesis and the transporter NTCP is both necessary and sufficient to explain BA composition and levels in male and female SPF mice (data not shown). This is in striking agreement to earlier findings which found an upregulation of BA synthesis (Cyp7b1) [28] as well as an elevated expression of the basolateral uptake transporter NTCP in female mice [29]. This finding is a first indication of the predictive capabilities of the computational model and generates confidence for further analyses.

Following parameter estimation, the final model adequately describes BA levels in various organs, in both male and female SPF mice (Figure 5A-B). Up to 60% of the experimental data are recapitulated within on standard deviation, 92% within a

two-fold variation, and only 12 of 156 data points were not captured accurately (Figure 5C-D). Even though the model describes a complex system and the measured data showed high variation, especially in the intestine, a good agreement between experimental data and model simulation was achieved.

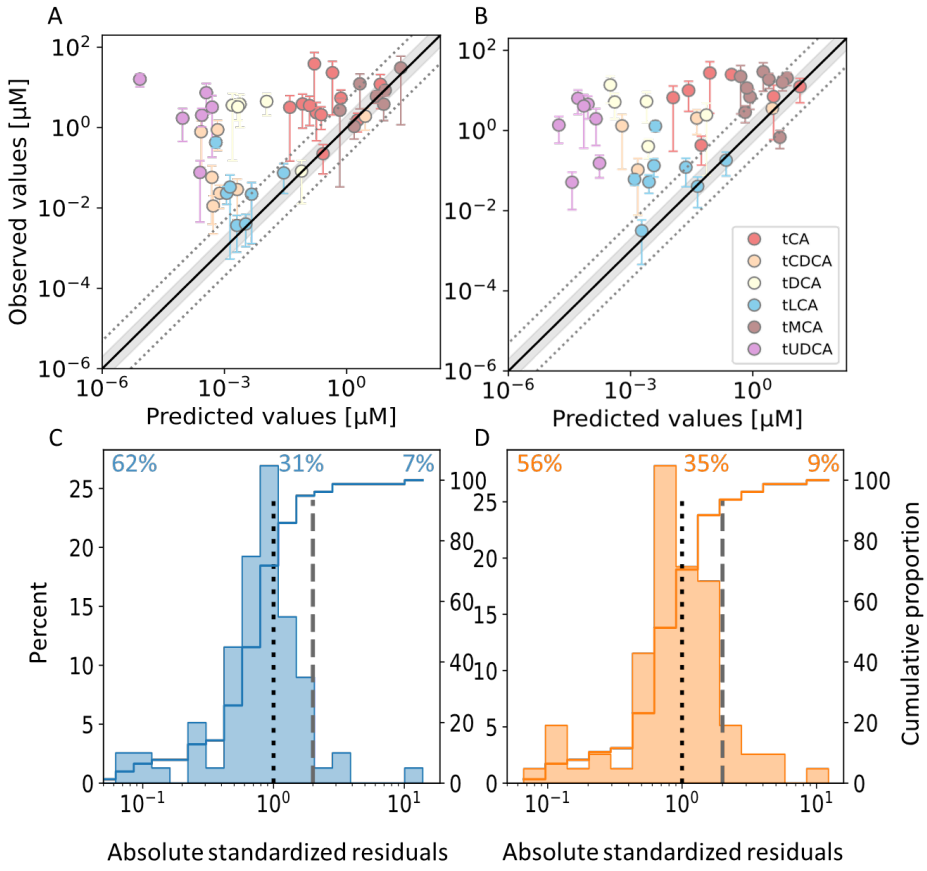

Fig 5. Model fit to data from SPF mice. Model simulations of concentration of bile acids in male (A) and female mice (B) against corresponding data points used for fitting. Only data points with a coefficient of variation below 1 are shown. Unity is shown as a solid black line shows unity, a two- and five-fold range between predicted and observed values is indicated as a gray area or with dotted lines, respectively. Error bars show the SD. Distribution of the absolute standardized residuals between model simulations and data of male (C) and female (D) mice (histogram) and the corresponding cumulative function (line). The dotted and dashed lines indicate differences between model simulation and measured data of one SD and two SD, respectively. Cumulative proportions of predictions that lie within one SD (top left, residuals left of dotted line), between one and two SD (top middle, residuals between dotted and dashed line) and above two SD (top right, residuals right of dashed line) of measured data are stated at the top of the panel.

Model qualification to germ-free mice

To further validate the computational model of SPF mice we next predicted BA levels in germ-free (GF) mice. To this end, we postulated that switching off the microbial

activity in the SPF model should be sufficient to describe BA metabolism and composition in GF mice. In a first step, any microbial reaction in the SPF model was therefore disabled. Resulting predictions recapitulated BA concentration in GF mice reasonably well (Figure 6A). About 59% of predicted concentrations fell within one standard deviation, 80% within a two-fold variation, and 15 predicted BA levels differed more strongly from the measured values (Figure 6B). Due to its mechanistic structure the physiology-based computational model of murine bile acid metabolism allows for the consideration of new scenarios as shown successfully for the case of GF mice.

In a next step, we aimed to verify whether the inclusion of additional physiological information for GF mice would further improve the agreement between model simulations and experimentally measured BA concentrations. Additional information about the physiology and intestinal transporter expression (Supplementary Figure S9 and S10) was hence included in the GF mouse model to better reproduce bile acid metabolism in these mice. By doing so, however, model predictions worsened slightly. Less predictions could be recapitulated within one SD, but 80% were still within two SD (Figure 7A) indicating that there are additional differences in BA metabolism between SPF and GF mice. Expression of the synthesizing enzymes CYP7A1, CYP27A1 and CYP7B1 were indeed shown to be elevated in germ-free mice [30–32]. However, increasing BA synthesis only yielded better model predictions by also allowing for differential regulation of other hepatic enzymes and processes. Upregulation of BSEP and downregulation of NTCP and MCA production from CDCA improved predictions only slightly (Figure 7B). The most accurate predictions of BA levels in GF mice could be obtained by allowing for reduced BA synthesis as well as differential regulation of hepatic processes. By doing so, 57% of predicted concentrations were within one SD, more than 80% within two, and only 12% were not explained well.

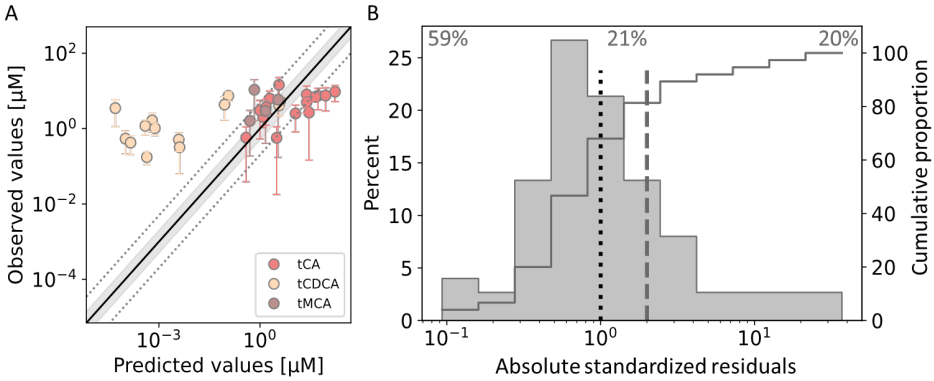

Fig 6. Model prediction of germ-free mice. Model predictions of concentration of bile acids in germ-free mice against corresponding data points used for fitting (A). Only data points with a coefficient of variation below 1 are shown. Unity is shown as a solid black line shows unity, a two- and five-fold range between predicted and observed values is indicated as a gray area or with dotted lines, respectively. Error bars represent the standard deviation. B) Distribution of the absolute standardized residuals model predictions (histogram) and the corresponding cumulative function (line). The dotted and dashed lines indicate differences between model simulation and measured data of one SD and two SD, respectively. Cumulative proportions of predictions that lie within one SD (top left, residuals left of dotted line), between one and two SD (top middle, residuals between dotted and dashed line) and above two SD (top right, residuals right of dashed line) of measured data are stated at the top of the panel.

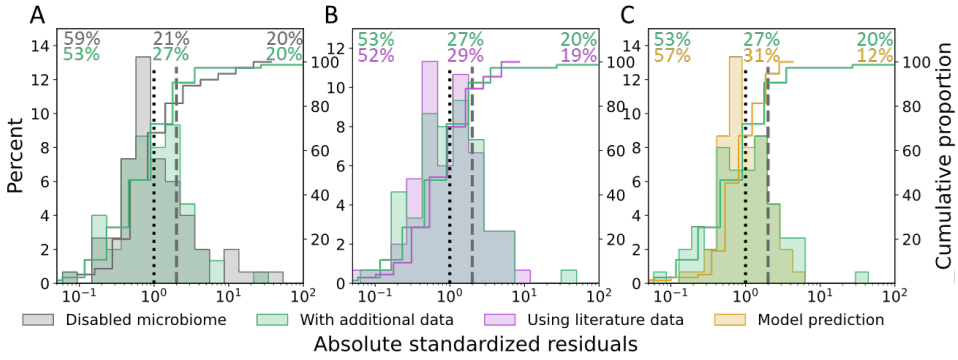

Fig 7. Model prediction of changes in germ-free mice. Comparison of different model variants for describing BA metabolism in germ-free mice by comparing the distribution of the absolute standardized residuals (histograms) and their corresponding cumulative function (lines). The dotted and dashed lines indicate differences between model simulation and measured data of one SD and two SD, respectively. Cumulative proportions of predictions that lie within one SD (top left, residuals left of dotted line), between one and two SD (top middle, residuals between dotted and dashed line) and above two SD (top right, residuals right of dashed line) of measured data are stated at the top of the panel. A) Comparison of a simple extrapolation of the base model by disabling any microbial reaction (grey) against a model variant with additional information about physiology and intestinal transporter expression (green). The latter was also tested against model variants that introduce further expressional changes in the liver (B) according to literature (pink) or (C) as suggested by the model itself (yellow).

Discussion and Conclusion

In this work, we established a physiology-based model of bile acid metabolism in mice. The model describes the systemic circulation, synthesis, hepatic and microbial conversions, and excretion of the most abundant BAs. It further addresses sex differences in BA concentration and composition that have been reported in the literature before but which were also prominent in our experimental studies. The model was carefully established and validated with an extensive data set specifically sampled from SPF mice, both male and female. Thus, the model integrates and contextualizes heterogeneous data including BA concentration in different organs, transporter expression along the gut segments, physiological parameters and microbial composition in the cecum. Of particular note, the model suggested upregulation of BA synthesis and the transporter NTCP in female SPF mice. This observation, which is excellent agreement to earlier findings [28, 29], is an independent outcome of the model development process and had not been considered as prior knowledge before.

Furthermore, the resulting model for SPF mice could be used to predict BA measurements in GF mice by specifically eliminating microbial processes. This is a strong indication for the overall model quality and provides confidence that the model can be used for further analyses and predictions. The model was next extended with additional information specifying physiological parameters and intestinal transporter expression in GF mice. We found that upregulation of BA synthesis, as reported in literature, is not sufficient to explain BA levels in GF mice but had to be complemented by additional expressional changes in the liver. Unrestricted model predictions however

suggested that BA synthesis might be downregulated. It remains to be investigated whether this discrepancy could be attributed to model inaccuracies or strain differences. This illustrates that the model can be applied for both extrapolation to unknown scenarios as well as contextualization of existing knowledge in a systemic manner, e.g., extrapolation to disease contexts or cross-species extrapolation.

Future analyses with the physiology based model will include structural revisions. In this version of the computational model, we included only the most abundant bile acid species but disregarded conjugation and sulfation. Our model can therefore not capture the full complexity of the BA pool and might introduce a systemic bias in our predictions as different BA species do not have the same kinetics [33]. Furthermore, we had to simplify the dynamic behaviour of BA circulation. In the computational model, all BAs are secreted directly into the duodenum. Thus, postprandial responses but also coprophagy, as a means of BA recycling [34, 35], were neglected as these effects are difficult to describe in mice. Consequently, the model cannot capture effects of the circadian rhythm as observed in other rodents [36–39]. Despite of these simplifications, it should be noted that the model is able to recapitulate BA composition and levels at the whole body level and account for sex-related differences in BA metabolism, both with good accuracy.

Alterations in BA composition and dynamics have been associated with a plethora of diseases. Compositional changes have been reported for inflammatory bowel disease (IBD), ulcerative colitis Crohn's Disease, liver cirrhosis, liver cancer, irritable bowel syndrome, short bowel syndrome, and obesity [2, 4, 5]. Impairments within the EHC of BA have been linked to cholestatic drug-induced liver injury, chronic liver disease, cholesterol gallstone disease, malabsorption, dyslipidemia and atherosclerosis [6–11]. In this context, the model could shed light on the complex interaction between pathophysiological alteration, such as physiological or expressional changes, microbial dysbiosis but also drug administration, and bile acid metabolism. .

Investigating the link between BA metabolism and their role in human disease, various animal models have been applied, including lamprey, skate, zebrafish, rat, mouse, hamster, rabbit, prairie dog, and monkey [40–42]. Of the small animal models, hamsters are most similar to humans regarding BA metabolism [43–45]; nevertheless, mice remain the most commonly utilized animal model to investigate human metabolism [12, 13]. Indicative of the difference between human and mice is the different bile acid composition [14, 46]. The human primary BAs are CA and CDCA, whereas mice produce CA as well as MCAs that are made from CDCA. MCAs are hydroxylated at the C-6 position, which alters their physicochemical as well as signalling properties. MCAs are more hydrophilic and less cytotoxic than other BAs and function as FXR antagonists instead of activating FXR signalling like other BAs [14]. Further differences relevant for BA metabolism can be found in the physiology of the GI tract [47–51], energy homeostasis [52] and the recycling of nutrients and bile acids through coprophagy [34, 35]. Therefore, extrapolation from mouse studies to humans for BA signalling or BA related diseases are difficult. The computational model developed in this work might support cross-species extrapolation due to the mechanistic structure of the underlying PBPK model [17]).

Lastly, the model can assist in optimizing experimental designs for mouse studies that aim to elucidate the complex behaviour of BAs in health and disease. This is especially relevant in the context of the principles of "3R" proposed by Russel and Burch in 1959 [53]: Reduction, Refinement and Replacement of animal testing. We believe that the here presented model can serve as a useful platform for model-aided investigation of BA metabolism in prospective studies.

Materials and Methods

Bile acid measurements

Sample preparation

First, x mg solid matrix were mixed with five times the μl amount of ACN:water (1:1, v/v) and homogenised with a TissueLyser II (30 Hz, 10 min; Retsch Qiagen). After a short centrifugation (2 min, 14000 rpm) 100 μl of the supernatant were added to 500 μl ACN:water:methanol (3:1:2, v/v/v) and the sample was vortexed for 5 min. After sonication (5 min) and centrifugation (14,000 rpm, 4°C, 5 min), 550 μl of the supernatant was transferred to a new tube and evaporated to dryness. The pellet was reconstituted in 100 μl 50% and 10 μL was used for analysis. For serum samples, 10 μl samples were used.

LC-MS analysis

The analysis was performed using the validated Bile Acid Kit (Biocrates Life Sciences, Innsbruck, Austria) as described in Pham et al. [54]. For that 10 μL of the native samples/sample extract were pipetted onto a 96 well sandwich filter plate and prepared according to manufacturer's instructions. For quantitation, 7 external calibration standards (each containing all 19 bile acids) and 10 isotope-labeled internal standards are used. A detailed list of metabolites is available at the manufacturer's homepage Kit (Biocrates Life Sciences AG, Innsbruck, Austria). The LC-MS/MS analysis carried out by MRM acquisition using a Waters Acquity UPLC System coupled with QTRAP 5500 (AB Sciex, Concord, Canada). MP A consisted of 10 mM ammonium acetate and 0.015% formic acid, while MP B was of a mixture of acetonitrile /methanol/water (65/30/5;v:v:v), 10 mM ammonium acetate and 0.015% formic acid. Data processing is carried out with the provided quantitation method Kit (Biocrates Life Sciences AG, Innsbruck, Austria).

Bile acid transporter expression

RNA isolation from homogenized tissue samples were performed using TRIzol reagent. Tissue homogenization was done using the FastPrep-24TM 5G from MP BiomedicalsTM. Isolated RNA was transcribed into cDNA using ReverseAid (Thermo Fisher) and RiboLock Inhibitor (Thermo Fisher). Quantitative PCR was done based on the use of taqman probes (Thermo Fisher) for the respective gene of interest (GOI). GOI expression was normalized to the expression of a housekeeping gene

Microbiota composition

Isolation of metagenomic DNA

DNA was isolated following a modified protocol according to Godon et al. [55]. Snap frozen samples were mixed with 600 μl stool DNA stabilizer (Stratec biomedical), thawed, and transferred into autoclaved 2-ml screw-cap tubes containing 500 mg 0.1 mm-diameter silica/zirconia beads. In a next step, 250 µl 4 M guanidine thiocyanate in 0.1 M Tris (pH 7.5) and 500 µl 5 % N-lauroyl sarcosine in 0.1 M PBS (pH 8.0) were added. Samples were then incubated at 70 °C and 700 rpm for 60 min. For cell disruption, a FastPrep® instrument (MP Biomedicals) fitted with a 24 × 2 ml cooling adaptor filled with dry ice was used. The program was run 3 times for 40 s at 6.5 M/s, and after each run, the cooling adapter was refilled with dry ice. An amount of 15 mg Polyvinylpyrrolidone (PVPP) was added and samples were vortexed, followed by 3 min

centrifugation at 15.000 x g and 4 °C. Approximately 650 μl of the supernatant were then transferred into a new 2 ml tube and was subsequently centrifuged again for 3 min at 15.000 x g and 4 °C. Then, 500 μl of the supernatant was transferred into a new 2 ml tube and 50 μg of RNase was added. After 20 minutes at 37 °C and 700 rpm, gDNA was isolated using the NucleoSpin® gDNA Clean-up Kit from Macherey-Nagel. Isolation was performed according to the manufacturer's protocol. DNA was eluted from columns twice using 40 μl Elution buffer and concentration was measured with NanoDrop® (Thermo Scientific). Samples were stored at -20 °C.

Illumina sequencing of 16S rRNA genes

Library preparation and sequencing were performed as described in detail previously [56] using an automation platform (Biomek400, Beckman Coulter). Briefly, the V3-V4 region of 16S rRNA genes was amplified in duplicates (25 cycles) following a two-step protocol [57] using primers 341F-785R [58]. After purification using the AMPure XP system (Beckman Coulter), sequencing was carried out with pooled samples in paired-end modus (PE300) using a MiSeq system (Illumina, Inc.) according to the manufacturer's instructions and 25% (v/v) PhiX standard library.

Computational methods

PBPK modelling

Software and calculations

The PBPK model of bile acid metabolism was established in PK-Sim® and further reactions and adjustments were done in MoBi® (Open Systems Pharmacology suite Version 11.150). Model simulations were performed using the ospsuite-R package in R (version 11.0.123). Parameter fitting was performed with the Monte Carlo algorithm implemented in the Open Systems Pharmacology suite. Residual calculation was set to linear and weights were derived from measured SD. Most reactions were defined as simple Michaelis-Menten kinetics, for BA synthesis a constant flux was assumed. Plotting and statistical testing was done with custom Python scripts.

16S rRNA amplicon data analysis

Data was analyzed with an updated version of a workflow previously described in [56]. Raw reads were processed using Integrated Microbial Next Generation Sequencing platform (www.imngs.org) [59] based on the UPARSE approach [60]. In brief, sequences were demultiplexed and trimmed to the first base with a quality score $\geq$10. The pairing, chimera filtering and OTU clustering (97% identity) was performed using USEARCH 11.0 [61]. Sequences that had less than 350 and more than 500 nucleotides and paired reads with an expected error ¿2 were excluded from the analysis. To avoid GC bias and non-random base composition, remaining reads were trimmed by fifteen nucleotides on each end. Operational taxonomic units (OTUs) were clustered at 97% sequence similarity, and only those with a relative abundance ¿0.25% in at least one sample were taken for further analysis. Sequence alignment and taxonomic classification was conducted with SINA 1.6.1, using the taxonomy of SILVA release 128 [62].

For assesssment of microbial richness, diversity and community structure, the selection of an appropriate method and subsequent normalization of OTU conut tables were performed as previously described in [63], using variant stabilization by the R package DESeq2 [64]. Calculation of α-diversity (observed species richness and Shannon effective index) and β-diversity (generalized UniFrac) indices was done using the Rhea pipline [65].

To assess potential differences in the relative abundance of bacterial genera between male and female mice, all OTUs were combined that were taxonomically assigned to the same genera or phyla. After filtering for a prevalence threshold of at least 10 counts in at least one sample, count tables were normalized using variant stabilization by DESeq2 [64]. To account for differences in sequencing depth between the samples, we used size factor correction. DESeq2 was also used for testing differential abundance of genera and phyla. Comparisons were performed using a Wald test to identify genera or phyla that showed changes in abundance between male and female mice. Results are reported as log2 fold changes and associated adjusted P[U+2010]values of the likelihood ratio test (Benjamini–Hochberg correction for the number of taxa and in addition the number of groups for the Wald test). Dendrograms were derived by hierarchical clustering using Ward's method where 1[U+2010]Pearson's correlation was used as the distance measure.

Acknowledgments

Supporting Information

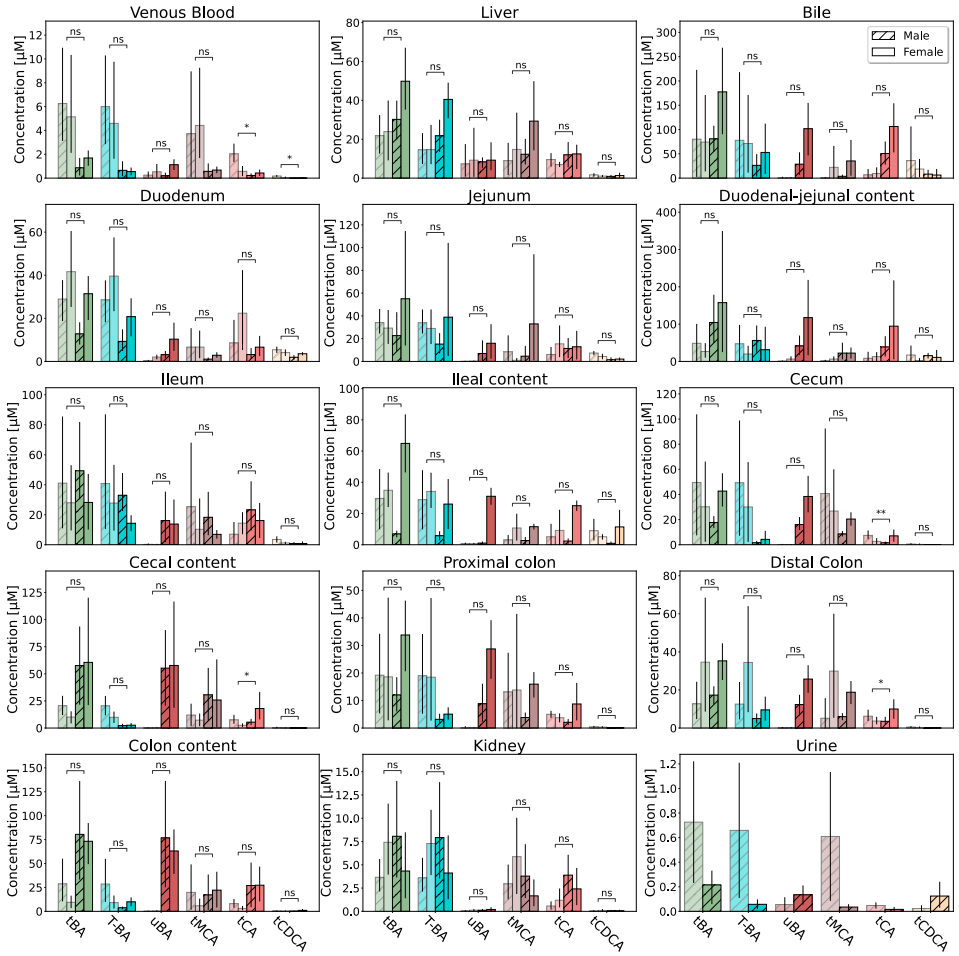

Fig 8. Bile acid levels in SPF and GF mice. Concentration of total BAs (tBA), tauro-conjugated BAs (T-BA), unconjugated BA (uBA), total cholic acid (tCA), total muricholic acids (tMCA) and total chenodeoxycholic acid (tCDCA) in various organs in male and female GF (pale coloration) and SPF mice (saturated coloration). Statistical differences were assessed by independent t-test. Statistical significance is marked with asterisks.

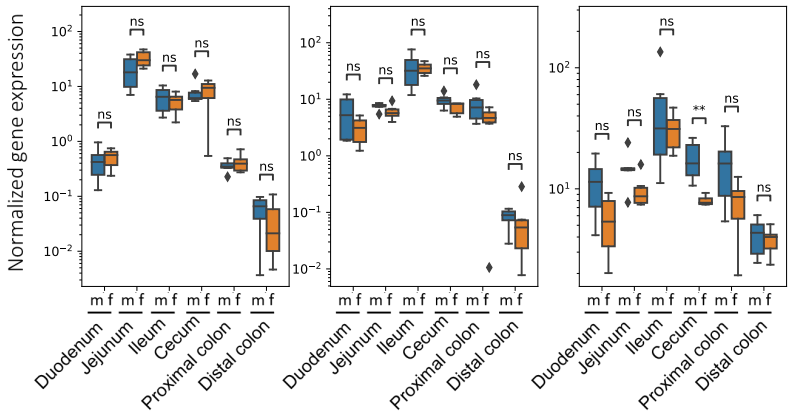

Fig 9. Sex-related differences in intestinal BA transporter expression. Assessment of sex-related differences in the expression of the BA transporters ASBT, OST-α and OST-β (from left to right) along the gut axis in male and female GF mice measured by qPCR. Statistical significance was assessed by Mann-Whitney U-test and statistical significance is marked with asterisks.

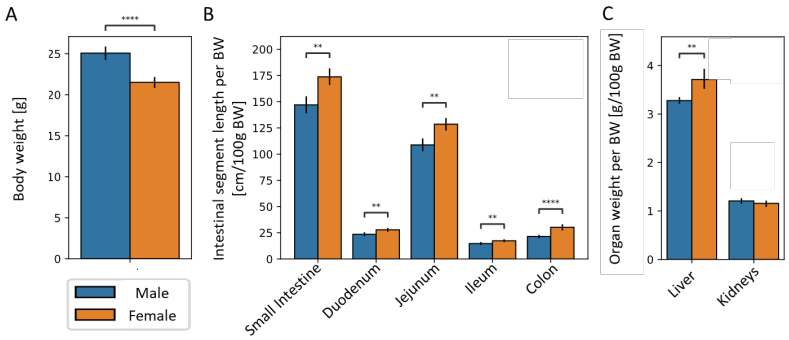

Fig 10. Physiological differences between male and female GF mice. Assessment of sex-related differences in body weight (A), length of intestinal segments (B) as well as weight of the liver and the kidneys (C) in GF mice. Significant differences were tested by two-way, independent t-test and significance was marked with asterisks.

References

1. Schaap FG, Trauner M, Jansen PLM. Bile acid receptors as targets for drug development. Nature Reviews Gastroenterology & Hepatology. 2014;11(1):55–67. doi:10.1038/nrgastro.2013.151.

2. Wahlström A, Sayin S, Marschall HU, Bäckhed F. Intestinal Crosstalk between Bile Acids and Microbiota and Its Impact on Host Metabolism. Cell Metabolism. 2016;24(1):41 – 50. doi:https://doi.org/10.1016/j.cmet.2016.05.005.

3. Ridlon JM, Harris SC, Bhowmik S, Kang DJ, Hylemon PB. Consequences of bile salt biotransformations by intestinal bacteria. Gut Microbes. 2016;7(1):22–39. doi:10.1080/19490976.2015.1127483.

4. Staley C, Weingarden AR, Khoruts A, Sadowsky MJ. Interaction of gut microbiota with bile acid metabolism and its influence on disease states. Applied microbiology and biotechnology. 2017;101(27888332):47–64.

5. Duboc H, Rajca S, Rainteau D, Benarous D, Maubert MA, Quervain E, et al. Connecting dysbiosis, bile-acid dysmetabolism and gut inflammation in inflammatory bowel diseases. Gut. 2013;62(4):531–539. doi:10.1136/gutjnl-2012-302578.

6. Wagner M, Trauner M. Recent advances in understanding and managing cholestasis [version 1; peer review: 2 approved]. F1000Research. 2016;5(705). doi:10.12688/f1000research.8012.1.

7. Jackson JP, Freeman KM, Friley WW, St Claire RL, Black C, Brouwer KR. Basolateral Efflux Transporters: A Potentially Important Pathway for the Prevention of Cholestatic Hepatotoxicity. Applied In Vitro Toxicology. 2016;2(4):207–216. doi:10.1089/aivt.2016.0023.

8. Castro ER, Rodrigues MPC. Cell Death and microRNAs in Cholestatic Liver Diseases: Update on Potential Therapeutic Applications; 2017. Available from: `http://www.eurekaselect.com/article/71155`.

9. Walters JRF, Tasleem AM, Omer OS, Brydon WG, Dew T, le Roux CW. A New Mechanism for Bile Acid Diarrhea: Defective Feedback Inhibition of Bile Acid Biosynthesis. Clinical Gastroenterology and Hepatology. 2009;7(11):1189–1194. doi:https://doi.org/10.1016/j.cgh.2009.04.024.

10. Degen LP, Phillips SF. Variability of gastrointestinal transit in healthy women and men. Gut. 1996;39(2):299–305. doi:10.1136/gut.39.2.299.

11. Guicciardi ME, Gores GJ. Bile acid-mediated hepatocyte apoptosis and cholestatic liver disease. Digestive and Liver Disease. 2002;34(6):387–392. doi:https://doi.org/10.1016/S1590-8658(02)80033-0.

12. Rosenthal N, Brown S. The mouse ascending: perspectives for human-disease models. Nature Cell Biology. 2007;9(9):993–999. doi:10.1038/ncb437.

13. Eppig JT. Mouse Genome Informatics (MGI) Resource: Genetic, Genomic, and Biological Knowledgebase for the Laboratory Mouse. ILAR Journal. 2017;58(1):17–41. doi:10.1093/ilar/ilx013.

14. Thakare R, Alamoudi JA, Gautam N, Rodrigues AD, Alnouti Y. Species differences in bile acids I. Plasma and urine bile acid composition. Journal of Applied Toxicology. 2018;38(10):1323–1335. doi:https://doi.org/10.1002/jat.3644.

15. Kuepfer L, Niederalt C, Wendl T, Schlender JF, Willmann S, Lippert J, et al. Applied Concepts in PBPK Modeling: How to Build a PBPK/PD Model. CPT: Pharmacometrics & Systems Pharmacology. 2016;5(10):516–531. doi:https://doi.org/10.1002/psp4.12134.

16. Schenk A, Ghallab A, Hofmann U, Hassan R, Schwarz M, Schuppert A, et al. Physiologically-based modelling in mice suggests an aggravated loss of clearance capacity after toxic liver damage. Scientific Reports. 2017;7(1):6224. doi:10.1038/s41598-017-04574-z.

17. Thiel C, Schneckener S, Krauss M, Ghallab A, Hofmann U, Kanacher T, et al. A systematic evaluation of the use of physiologically based pharmacokinetic modeling for cross-species extrapolation. Journal of pharmaceutical sciences. 2015;104:191–206.

18. Krauss M, Schaller S, Borchers S, Findeisen R, Lippert J, Kuepfer L. Integrating Cellular Metabolism into a Multiscale Whole-Body Model. PLOS Computational Biology. 2012;8(10):1–13. doi:10.1371/journal.pcbi.1002750.

19. Wahlström A, Al-Dury S, Ståhlman M, Bäckhed F, Marschall HU. Cyp3a11 is not essential for the formation of murine bile acids. Biochemistry and Biophysics Reports. 2017;10:70 – 75. doi:https://doi.org/10.1016/j.bbrep.2017.02.011.

20. Jung D, Inagaki T, Gerard RD, Dawson PA, Kliewer SA, Mangelsdorf DJ, et al. FXR agonists and FGF15 reduce fecal bile acid excretion in a mouse model of bile acid malabsorption. Journal of lipid research. 2007;48(17823457):2693–2700.

21. Yu L, Li-Hawkins J, Hammer RE, Berge KE, Horton JD, Cohen JC, et al. Overexpression of ABCG5 and ABCG8 promotes biliary cholesterol secretion and reduces fractional absorption of dietary cholesterol. The Journal of Clinical Investigation. 2002;110(5):671–680. doi:10.1172/JCI16001.

22. Dawson PA, Haywood J, Craddock AL, Wilson M, Tietjen M, Kluckman K, et al. Targeted deletion of the ileal bile acid transporter eliminates enterohepatic cycling of bile acids in mice. The Journal of biological chemistry. 2003;278(12819193):33920–33927.

23. Marschall HU, Wagner M, Bodin K, Zollner G, Fickert P, Gumhold J, et al. Fxr(-/-) mice adapt to biliary obstruction by enhanced phase I detoxification and renal elimination of bile acids. Journal of lipid research. 2006;47(16327028):582–592.

24. Tannock GW, Dashkevicz MP, Feighner SD. Lactobacilli and bile salt hydrolase in the murine intestinal tract. Applied and Environmental Microbiology. 1989;55(7):1848–1851.

25. Wishart DS, Guo A, Oler E, Wang F, Anjum A, Peters H, et al. HMDB 5.0: the Human Metabolome Database for 2022. Nucleic Acids Research. 2021;50(D1):D622–D631. doi:10.1093/nar/gkab1062.

26. Heuman DM, Hylemon PB, Vlahcevic ZR. Regulation of bile acid synthesis. III. Correlation between biliary bile salt hydrophobicity index and the activities of enzymes regulating cholesterol and bile acid synthesis in the rat. Journal of lipid research. 1989;30:1161–71.

27. Watanabe M, Horai Y, Houten SM, Morimoto K, Sugizaki T, Arita E, et al. Lowering bile acid pool size with a synthetic farnesoid X receptor (FXR) agonist induces obesity and diabetes through reduced energy expenditure. The Journal of biological chemistry. 2011;286(21632533):26913–26920.

28. Link JC, Xuqi C, Christopher P, Borja Mark S, Bradley H, Oda Michael N, et al. Increased High-Density Lipoprotein Cholesterol Levels in Mice With XX Versus XY Sex Chromosomes. Arteriosclerosis, Thrombosis, and Vascular Biology. 2015;35(8):1778–1786. doi:10.1161/atvbaha.115.305460.

29. Cheng X, Buckley D, Klaassen CD. Regulation of hepatic bile acid transporters Ntcp and Bsep expression. Biochemical pharmacology. 2007;74:1665–76.

30. Wahlström A, Kovatcheva-Datchary P, Ståhlman M, Khan MT, Bäckhed F, Marschall HU. Induction of farnesoid X receptor signaling in germ-free mice colonized with a human microbiota. Journal of lipid research. 2017;58:412–419.

31. Sayin S, Wahlström A, Felin J, Jäntti S, Marschall HU, Bamberg K, et al. Gut Microbiota Regulates Bile Acid Metabolism by Reducing the Levels of Tauro-beta-muricholic Acid, a Naturally Occurring FXR Antagonist. Cell Metabolism. 2013;17(2):225 – 235. doi:https://doi.org/10.1016/j.cmet.2013.01.003.

32. Li F, Jiang C, Krausz KW, Li Y, Albert I, Hao H, et al. Microbiome remodelling leads to inhibition of intestinal farnesoid X receptor signalling and decreased obesity. Nature communications. 2013;4:2384.

33. Setchell KD, Rodrigues CM, Clerici C, Solinas A, Morelli A, Gartung C, et al. Bile acid concentrations in human and rat liver tissue and in hepatocyte nuclei. Gastroenterology. 1997;112:226–35.

34. Sakaguchi E. Digestive strategies of small hindgut fermenters. Animal Science Journal. 2003;74(5):327–337. doi:https://doi.org/10.1046/j.1344-3941.2003.00124.x.

35. Klaasen HLBM, Koopman JP, Scholten PM, Brink MEVD, Theeuwes AGM. Effect of Preventing Coprophagy on Colonisation by Segmented Filamentous Bacteria in the Small Bowel of Mice. Microbial Ecology in Health and Disease. 1990;3(2):99–103. doi:10.3109/08910609009140123.

36. Ho KJ. Circadian distribution of bile acid in the enterohepatic circulatory system in hamsters. Journal of lipid research. 1976;17:600–4.

37. Ho KJ. Circadian distribution of bile acids in the enterohepatic circulatory system in rats. The American journal of physiology. 1976;230:1331–5.

38. Zhang YKJ, Guo GL, Klaassen CD. Diurnal variations of mouse plasma and hepatic bile acid concentrations as well as expression of biosynthetic enzymes and transporters. PloS one. 2011;6:e16683.

39. Eggink HM, Oosterman JE, de Goede P, de Vries EM, Foppen E, Koehorst M, et al. Complex interaction between circadian rhythm and diet on bile acid homeostasis in male rats. Chronobiology International. 2017;34(10):1339–1353. doi:10.1080/07420528.2017.1363226.

40. Baghdasaryan A, Fuchs CD, Österreicher CH, Lemberger UJ, Halilbasic E, Påhlman I, et al. Inhibition of intestinal bile acid absorption improves cholestatic liver and bile duct injury in a mouse model of sclerosing cholangitis. Journal of Hepatology. 2016;64(3):674–681. doi:https://doi.org/10.1016/j.jhep.2015.10.024.

41. Woolbright BL, Jaeschke H. Novel insight into mechanisms of cholestatic liver injury. World journal of gastroenterology. 2012;18:4985–93.

42. Jansen PLM, Ghallab A, Vartak N, Reif R, Schaap FG, Hampe J, et al. The ascending pathophysiology of cholestatic liver disease. Hepatology. 2017;65(2):722–738. doi:https://doi.org/10.1002/hep.28965.

43. Dietschy J, Turley S, Spady D. Role of liver in the maintenance of cholesterol and low density lipoprotein homeostasis in different animal species, including humans. Journal of Lipid Research. 1993;34(10):1637–1659. doi:https://doi.org/10.1016/S0022-2275(20)35728-X.

44. Gurantz D, Hofmann AF. Influence of bile acid structure on bile flow and biliary lipid secretion in the hamster. American Journal of Physiology-Gastrointestinal and Liver Physiology. 1984;247(6):G736–G748. doi:10.1152/ajpgi.1984.247.6.G736.

45. van Golen RF, Olthof PB, de Haan LR, Coelen RJ, Pechlivanis A, de Keijzer MJ, et al. The pathophysiology of human obstructive cholestasis is mimicked in cholestatic Gold Syrian hamsters. Biochimica et Biophysica Acta (BBA) - Molecular Basis of Disease. 2018;1864(3):942–951. doi:https://doi.org/10.1016/j.bbadis.2017.11.022.

46. Li J, Dawson PA. Animal models to study bile acid metabolism. Biochimica et Biophysica Acta (BBA) - Molecular Basis of Disease. 2019;1865(5):895 – 911. doi:https://doi.org/10.1016/j.bbadis.2018.05.011.

47. Hugenholtz F, de Vos WM. Mouse models for human intestinal microbiota research: a critical evaluation. Cellular and molecular life sciences : CMLS. 2018;75(29124307):149–160. doi:10.1007/s00018-017-2693-8.

48. Ghoshal NG, Bal HS. Comparative morphology of the stomach of some laboratory mammals. Laboratory animals. 1989;23:21–9.

49. McConnell EL, Basit AW, Murdan S. Measurements of rat and mouse gastrointestinal pH, fluid and lymphoid tissue, and implications for in-vivo experiments. The Journal of pharmacy and pharmacology. 2008;60:63–70.

50. Booijink CCGM, Zoetendal EG, Kleerebezem M, de Vos WM. Microbial communities in the human small intestine: coupling diversity to metagenomics. Future microbiology. 2007;2:285–95.

51. Sheridan WG, Lowndes RH, Young HL. Intraoperative tissue oximetry in the human gastrointestinal tract. American journal of surgery. 1990;159:314–9.

52. Kleiber M. Metabolic turnover rate: a physiological meaning of the metabolic rate per unit body weight. Journal of theoretical biology. 1975;53:199–204.

53. Russell WMS, Burch RL. The principles of humane experimental technique. Methuen; 1959.

54. Pham HT, Arnhard K, Asad YJ, Deng L, Felder TK, St John-Williams L, et al. Inter-Laboratory Robustness of Next-Generation Bile Acid Study in Mice and Humans: International Ring Trial Involving 12 Laboratories. The Journal of Applied Laboratory Medicine. 2016;1(2):129–142. doi:10.1373/jalm.2016.020537.

55. Godon JJ, Zumstein E, Dabert P, Habouzit F, Moletta R. Molecular microbial diversity of an anaerobic digestor as determined by small-subunit rDNA sequence analysis. Applied and environmental microbiology. 1997;63:2802–13.

56. Lagkouvardos I, Kläring K, Heinzmann SS, Platz S, Scholz B, Engel KH, et al. Gut metabolites and bacterial community networks during a pilot intervention study with flaxseeds in healthy adult men. Molecular nutrition & food research. 2015;59:1614–28.

57. Berry D, Ben Mahfoudh K, Wagner M, Loy A. Barcoded primers used in multiplex amplicon pyrosequencing bias amplification. Applied and environmental microbiology. 2011;77:7846–9.

58. Klindworth A, Pruesse E, Schweer T, Peplies J, Quast C, Horn M, et al. Evaluation of general 16S ribosomal RNA gene PCR primers for classical and next-generation sequencing-based diversity studies. Nucleic acids research. 2013;41:e1.

59. Lagkouvardos I, Joseph D, Kapfhammer M, Giritli S, Horn M, Haller D, et al. IMNGS: A comprehensive open resource of processed 16S rRNA microbial profiles for ecology and diversity studies. Scientific Reports. 2016;6(1):33721. doi:10.1038/srep33721.

60. Edgar RC. UPARSE: highly accurate OTU sequences from microbial amplicon reads. Nature methods. 2013;10:996–8.

61. Edgar RC. Search and clustering orders of magnitude faster than BLAST. Bioinformatics (Oxford, England). 2010;26:2460–1.

62. Pruesse E, Peplies J, Glöckner FO. SINA: accurate high-throughput multiple sequence alignment of ribosomal RNA genes. Bioinformatics (Oxford, England). 2012;28:1823–9.

63. de Wert LA, Rensen SS, Soons Z, Poeze M, Bouvy ND, Penders J. The cutaneous microbiome in hospitalized patients with pressure ulcers. Scientific reports. 2020;10:5963.

64. Love MI, Huber W, Anders S. Moderated estimation of fold change and dispersion for RNA-seq data with DESeq2. Genome biology. 2014;15:550.

65. Lagkouvardos I, Fischer S, Kumar N, Clavel T. Rhea: a transparent and modular R pipeline for microbial profiling based on 16S rRNA gene amplicons. PeerJ. 2017;5:e2836.